^{11}C-PABA as a PET Radiotracer for Functional Renal Imaging: Preclinical and First-in-Human Study

Camilo A. Ruiz-Bedoya*[1,2], Alvaro A. Ordonez*[1,2], Rudolf A. Werner[3], Donika Plyku[4], Mariah H. Klunk[1,2], Jeff Leal[4], Wojciech G. Lesniak[4], Daniel P. Holt[4], Robert F. Dannals[4], Takahiro Higuchi[5,6], Steven P. Rowe[4], and Sanjay K. Jain[1,2,4]

[1]Center for Infection and Inflammation Imaging Research, Johns Hopkins University School of Medicine, Baltimore, Maryland; [2]Department of Pediatrics, Johns Hopkins University School of Medicine, Baltimore, Maryland; [3]Department of Nuclear Medicine, Hannover Medical School, Hannover, Germany; [4]Russell H. Morgan Department of Radiology and Radiological Sciences, Johns Hopkins University School of Medicine, Baltimore, Maryland; [5]Okayama University Graduate School of Medicine, Dentistry and Pharmaceutical Sciences, Okayama, Japan; and [6]Department of Nuclear Medicine, University Hospital, University of Würzburg, Würzburg, Germany

para-Aminobenzoic acid (PABA) has been previously used as an exogenous marker to verify completion of 24-h urine sampling. Therefore, we hypothesized that PABA radiolabeled with ^{11}C might allow high-quality dynamic PET of the kidneys with less radiation exposure than other agents because of its shorter biologic and physical half-life. We evaluated if ^{11}C-PABA can visualize renal anatomy and quantify function in healthy rats and rabbits and in a first-in-humans study on healthy volunteers. **Methods:** Healthy rats and rabbits were injected with ^{11}C-PABA intravenously. Subsequently, dynamic PET was performed, followed by postmortem tissue-biodistribution studies. ^{11}C-PABA PET was directly compared with the current standard, ^{99m}Tc-mercaptoacetyltriglycin, in rats. Three healthy human subjects also underwent dynamic PET after intravenous injection of ^{11}C-PABA. **Results:** In healthy rats and rabbits, dynamic PET demonstrated a rapid accumulation of ^{11}C-PABA in the renal cortex, followed by rapid excretion through the pelvicalyceal system. In humans, ^{11}C-PABA PET was safe and well tolerated. There were no adverse or clinically detectable pharmacologic effects in any subject. The cortex was delineated on PET, and the activity gradually transited to the medulla and then pelvis with high spatiotemporal resolution. **Conclusion:** ^{11}C-PABA demonstrated fast renal excretion with a very low background signal in animals and humans. These results suggest that ^{11}C-PABA might be used as a novel radiotracer for functional renal imaging, providing high-quality spatiotemporal images with low radiation exposure.

Key Words: PABA; renal imaging; PET; renography; translational science

The use of molecular imaging to evaluate renal function is a field that has been an evolving for many decades (*1*). The initial approaches were based on radiolabeled agents with high renal clearance, focusing on ^{99m}Tc-radiopharmaceuticals (e.g., ^{99m}Tc-mercaptoacetyltriglycin [^{99m}Tc-MAG3]) and planar γ-cameras. Although these techniques are still widely used in clinical practice, they have some major limitations in that they provide only 2-dimensional information, with a concomitant lack of accurate anatomic correlation, low spatial resolution, and low signal-to-background ratio. The soft tissue attenuation may also reduce diagnostic accuracy and limit reliable quantification (*2*). Implementation of SPECT for renal imaging led to improvements in image contrast and spatial resolution. However, in recent years there has been a shift toward the development of PET renal imaging agents. PET offers multiple advantages such as 3-dimensional dynamic visualization of the kidneys without organ overlap, a higher sensitivity and signal-to-background ratio, and absolute camera-based quantification with higher counts. PET allows administration of much lower doses of radioactivity and provides higher-accuracy measurements of regional radiopharmaceutical tissue concentrations (*2–4*). Novel agents for PET renal imaging that have shown promise include ethylenediaminetetraacetic acid labeled with ^{68}Ga, fluorodeoxysorbitol labeled with ^{18}F, nonpeptide angiotensin 1 antagonist labeled with ^{11}C, ^{11}C-acetate, *para*-^{18}F-aminohippurate, and Re(CO)$_3$-*N*-(^{18}F-fluoroethyl)iminodiacetic acid, which reflects tubular function (*2–8*).

para-Aminobenzoic acid (PABA) is a nontoxic B-complex vitamin with fast renal excretion that has been used since the 1980s as an exogenous marker to verify the completion of 24-h urine sampling (*9,10*). Although PABA undergoes hepatic metabolism by phase II conjugation via *N*-acetyltransferase 1 and glycine conjugation, all its metabolites are renally excreted (*11,12*). By targeting the incorporation of PABA into the folate synthesis of bacteria, with low uptake in mammalian tissues and rapid renal elimination, investigators are developing radiolabeled analogs of PABA for bacteria-specific imaging (*13–15*). We hypothesized that the high renal concentration, excretion, and performance of ^{11}C-PABA, as well as the potential for low radiation exposure, would be valuable characteristics for a renal imaging agent. In this article, we describe ^{11}C-PABA PET renal imaging in 2 healthy animal species and a first-in-humans study on healthy volunteers.

MATERIALS AND METHODS

All animal protocols were approved by the Johns Hopkins University Biosafety, Radiation Safety, and Animal Care and Use Committees.

Human studies were approved by the Johns Hopkins Institutional Review Board and performed under the auspices of the Radioactive Drug Research Committee program.

Synthesis of ^{11}C-PABA

^{11}C-PABA was synthesized as a sterile, pyrogen-free solution with high radiochemical purity and high specific activity (163.7 ± 40.9 GBq/μmol) using current good manufacturing practices at the Johns Hopkins Hospital PET center ([16]).

Animal Studies

Healthy Wistar rats (Charles River Laboratories) weighing 301.5 ± 33.2 g (3 females, 1 male) were injected with 22.3 ± 3.9 MBq of ^{11}C-PABA through a tail-vein catheter, and dynamic PET was performed immediately afterward using a nanoScan PET/CT device (Mediso). The acquisition parameters were fifteen 1-min and six 5-min frames, for a total acquisition of 45 min. Healthy New Zealand White rabbits (Charles River Laboratories) weighing 3.0 ± 0.2 kg (2 females) were intravenously injected with 51.9 ± 3.9 MBq of ^{11}C-PABA, followed by a 40-min dynamic PET scan using the nanoScan PET/CT device. The acquisition parameters were fifteen 1-min and five 6-min frames, for a total acquisition of 40 min. A CT scan for anatomic coregistration was also acquired for all animals. Quantitative analysis was performed by placing 7 volumes of interest using the CT images as a reference within the kidneys: outer layer (corresponding to renal cortex), inner layer (corresponding to renal pelvis), intermediate layer (corresponding to renal medulla), and bladder (only in rats). (The analyses for all the remaining volumes of interest are mentioned and plotted on Supplemental Fig. 1.) Renal perfusion was observed by visual assessment of ^{11}C-PABA transit through the abdominal aorta after the injection. The images were analyzed using VivoQuant, version 4.0 (Invicro), and visualized using Amide, version 1.0.4. Maximal parenchymal uptake is represented as T_{max}, which is the time from injection to peak activity on the renogram. The half-life is represented as $T_{1/2}$, which is the time from T_{max} to a 50% decrease. The relative renal uptake of the right and left kidneys is expressed as the percentage of the total uptake.

Postmortem Tissue Biodistribution

Four additional healthy female Wistar rats (weighing 235.1 ± 28.9 g) were given a simultaneous intravenous injection of 26.5 ± 1.5 MBq of ^{11}C-PABA and 18.1 ± 0.6 MBq of ^{99m}Tc-MAG3 (Cardinal Health). The animals were sacrificed 30 min afterward, the tissues were harvested, and the associated radioactivity was quantified using an automated γ-counter (1282 Compugamma γ-Counter CS; LKB Wallac). The measurements for ^{99m}Tc-MAG3 were performed 2 h after those for ^{11}C-PABA. The tissue biodistribution data are presented as percentage injected dose per gram of tissue.

Dosimetry

Four healthy mice (CBA/j; Jackson Laboratory) were injected with 47.73 ± 2.59 MBq of ^{11}C-PABA through a tail-vein catheter, and dynamic PET was performed immediately afterward over 85 min as described in the "Animal Studies" section. The activity concentrations from the 4 mice were determined and used to calculate human organ-absorbed doses and time-integrated activity coefficients using the MIRD S-value methodology as implemented in the OLINDA/EXM software package ([17–20]).

The PET images were first coregistered to the CT images. Partial regions of interest were drawn on the CT images of a selection of mouse organs (brain, heart, lungs, liver, muscle, large intestine, and bone marrow) to obtain the activity concentration at 18 measured time-points after injection (0, 5, 10, 15, 20, 25, 30, 35, 40, 45, 50, 55, 60, 65, 70, 75, 80, and 85 min). Whole-organ contours were drawn to measure the activity in the kidneys and bladder. The mean activity concentration (Bq/mL) and activity (Bq) were recorded for each mouse. The measured activity was decay-corrected to the time at the start of the acquisition (T0).

To account for physical decay of ^{11}C as needed for dosimetry calculations, the effective activity concentration was obtained as follows:

$$\text{Effective activity concentration}$$
$$= \text{biologic activity concentration} \times \exp(-\lambda^{11}C \times time),$$

where the physical λ of ^{11}C is calculated as $\ln(2)/T_{1/2}$ ($T_{1/2}$ is 20.33 h for ^{11}C).

The effective activity concentrations were divided by the injected activities in each mouse to obtain the fraction of injected activity per cubic centimeter. From the data for the 4 mice, this fraction was calculated, multiplied by the mouse organ volume based on the 4-dimensional mouse whole-body phantom ([19]), and then divided by the mouse organ mass for the 25-g reference mouse model ([19]) to obtain the average fraction of injected activity per gram for each organ.

The following equation was used to convert mouse activity data to human activity data:

$$[FIA/organ]_H = [FID/g]_M \times OM_H \times [TBM_M/TBM_H],$$

where FIA is the fraction of injected activity (activity inside the syringe before injection), FID is the fraction of injected dose (effective dose administered), OM_H is the human organ mass (using organ masses from OLINDA EXM), TBM_M is the mouse total-body mass (set to 19.7 g), and TBM_H is the human total-body mass (set to 73.7 kg, from the OLINDA EXM compilation of organ masses).

The human total heart mass (tissue plus blood in chambers, 620 g for women and 840 g for men) was used when converting mouse heart time–activity data to human heart time–activity data. The human bladder time–activity data were obtained using both human bladder tissue only (bladder wall, 35.90 g for women and 47.60 g for men) and bladder plus contents (bladder contents, 200 g for both men and women) ([20]).

The activity in the remainder of the body for the mouse was calculated by subtracting the measured whole-body (whole field of view) activity from the sum of the activity data of the measured organs. For each measured time-point in the dynamic PET data, the ratio of the body-remainder activity to the whole-body activity was calculated for the average mouse time–activity data. The calculated human organ time–activity data were summed and multiplied by the ratio of the body-remainder activity to the whole-body activity derived from the mouse data in order to estimate body-remainder activity in humans.

The MIRD Committee S-value methodology ([18]), as implemented in the OLINDA/EXM software package ([17]), was used to perform the absorbed dose calculations. The S-value methodology provides the absorbed dose to a target tissue as the sum of dose contributions from all radioactivity-containing (source) tissues. The S value is usually obtained by Monte Carlo simulation based on a standard or reference geometry of the patient and the decay characteristics and emission spectrum of the radionuclide. S values for a number of source and target tissue combinations and a large number of radionuclides have been previously incorporated into OLINDA/EXM. Once the absorbed dose for a series of organs is obtained, the effective dose can be calculated using tissue-weighting factors.

Time–activity graphs were obtained for the following human organs (both male and female) based on the provided murine data: brain, heart, lungs, liver, muscle, large intestine, bladder, kidneys, and bone

TABLE 1
Characteristics of Human Subjects

Subject no.	Sex	Age (y)	BMI (kg/m²)	Creatinine (mg/dL)	GFR (mL/min/ 1.73 m²)	Albumin (g/dL)	Injected ¹¹C-PABA dose (MBq)
1	M	23	21	0.8	154	4.9	685.6
2	M	25	20	0.8	143	4.8	671.2
3	F	30	21	0.7	134	4.8	683.4

BMI = body mass index; GFR = glomerular filtration rate.

marrow. These graphs were fit using a monoexponential function and were integrated from 0 to infinity to obtain the time-integrated activity coefficient, or residence time.

Adult female and male phantoms were used, and absorbed-dose calculations were performed for ¹¹C using the calculated time-integrated activity coefficients for the given source organs as input into OLINDA/EXM. The absorbed dose to the urinary bladder was estimated using the bladder model as implemented in OLINDA/EXM (17), with a biologic half-life of 1.6 h for PABA and a bladder voiding period of 1 h.

FIGURE 1. ¹¹C-PABA PET/CT renal imaging in healthy rats. (A) Coronal dynamic ¹¹C-PABA PET images of right kidney from representative rat show rapid cortical uptake after 2 min, followed by rapid clearance through pelvicalyceal system. (B) Maximum-intensity-projection ¹¹C-PABA PET/CT images show abdominal aorta and iliac arteries 60 s after injection, as well as high activity in bladder (Bl) after 20 min, with low background signal in other tissues. (C) Average ¹¹C-PABA time–activity curves for kidneys and bladder. Data are mean (solid lines) and SD (shaded areas) (n = 4). %ID = percentage injected dose.

First-in-Humans Study

Three healthy volunteers (2 male, 1 female) at least 18 y old (age range, 23–30 y) were recruited from an ongoing first-in-humans ¹¹C-PABA PET study at the Johns Hopkins Hospital (Table 1). The Johns Hopkins Institutional Review Board approved the study, and all subjects gave written informed consent. The prestudy evaluation included a medical history, a physical examination with vital signs, and laboratory tests (a comprehensive metabolic panel, including alkaline phosphatase, total bilirubin, liver transaminase levels, and renal function [blood urea nitrogen and creatinine]). The eligibility criterion was a laboratory evaluation showing normal liver function within 28 d before enrollment. Female subjects were screened for pregnancy and excluded if pregnant or lactating. Other exclusion criteria included subjects with hypertension, diabetes mellitus, a body mass index lower than 18.5 kg/m² or higher than 30 kg/m², a family history of renal disease, or a urinary tract infection in the prior 6 mo. Subjects who had been treated with an investigational drug, an investigational biologic, or an investigational therapeutic device within 30 d before radiotracer administration were also excluded.

The subjects were injected with ¹¹C-PABA (mean administered activity, 680.1 ± 7.8 MBq [range, 671.2–685.6 MBq]; mean administered mass, 593.3 ± 142.9 ng [range, 470–750 ng]), after which a 30-min dynamic single-bed-position PET scan was obtained on a Biograph mCT 128-slice PET/CT device (Siemens Healthineers) operating in 3-dimensional emission mode. The subjects were positioned supine with their arms above their head, and a scout scan encompassing the abdomen was used to locate the kidneys for the PET acquisition. The acquisition area included both kidneys at a single bed position. A 30-min list-mode acquisition was started just before radiotracer injection. The reconstructed images consisted of 10 frames for 5 s, 20 frames for 15 s, and 25 frames for 60 s. A low-dose CT scan was subsequently acquired for anatomic localization and attenuation correction. The subjects were asked to empty their bladder before injection and after
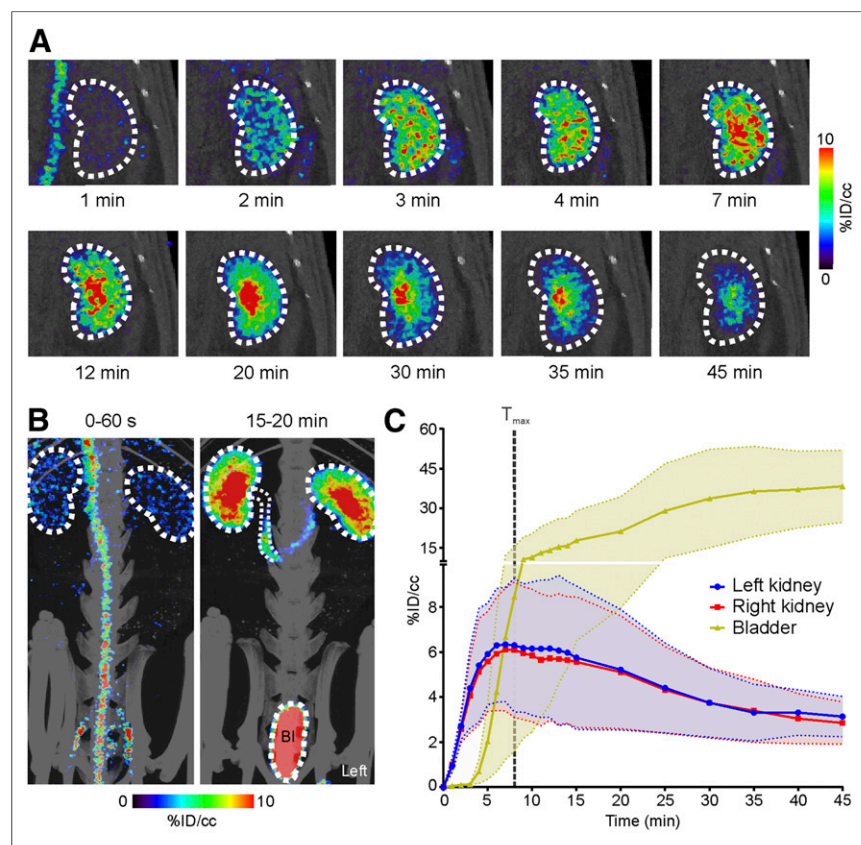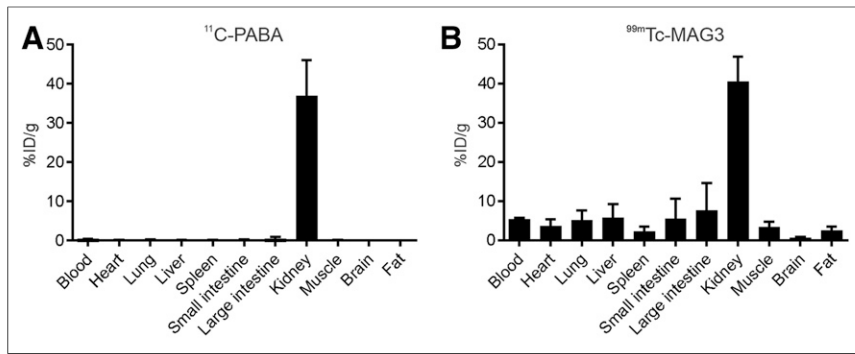
FIGURE 2. ^{11}C-PABA and ^{99m}Tc-MAG3 tissue biodistribution in rats. Healthy rats received simultaneous intravenous injections of ^{11}C-PABA and ^{99m}Tc-MAG3 and were killed 30 min afterward. ^{99m}Tc-MAG3 counts were determined 2 h after ^{11}C-PABA counts, when signal from ^{11}C (physical half-life, 20 min) would have completely decayed. (A) Biodistribution of ^{11}C-PABA was primarily within kidneys, with very low activity in all other measured organs. (B) Conversely, biodistribution of ^{99m}Tc-MAG3 had higher background activity. Data are mean and SD ($n = 4$).

analyzed with Mirada XD (Mirada Medical) and PMOD (PMOD Technologies) for dynamic quantification. Amide, version 1.0.4, and Imager-4D (21) were used for data visualization. The subjects were followed up by telephone 25 d after imaging to assess for any side effects or other issues.

Statistical Analysis

For the animal imaging studies, data are represented on a linear scale as the average of the percentage injected dose per cubic centimeter ± SD. Data for postmortem biodistribution are represented as percentage injected dose per gram of tissue. For human imaging studies, data are represented on a linear scale as average SUV ± SD. All statistical analyses were performed using Prism, version 8 (GraphPad Software).
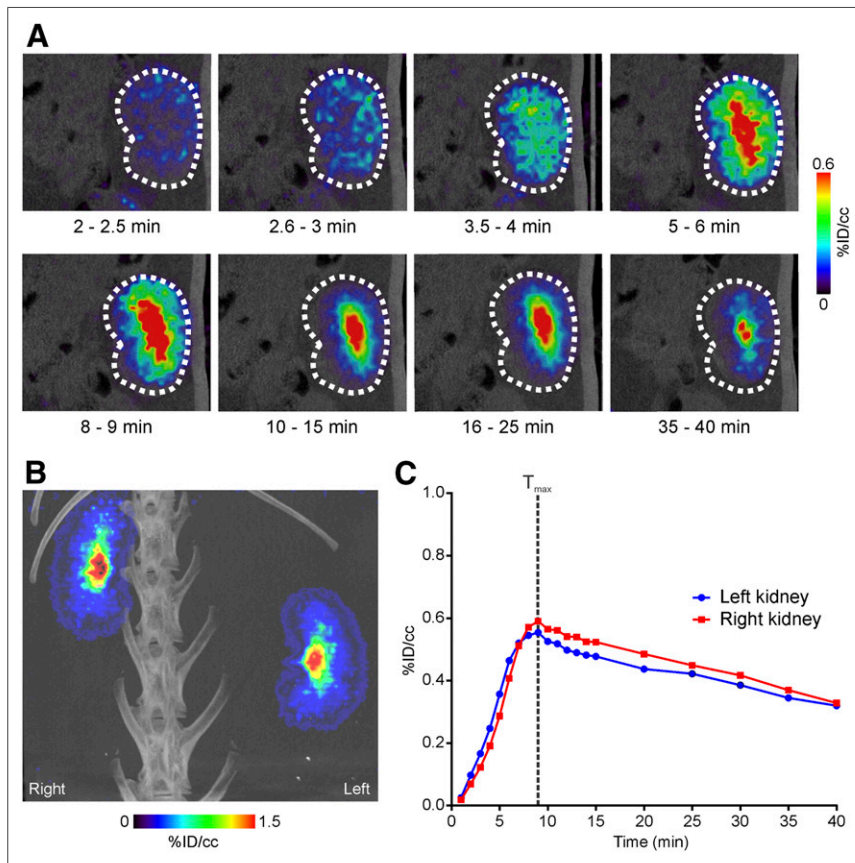
the imaging was completed. To perform the quantitative analysis, 7 volumes of interest were manually drawn using the CT images as a reference as described for the preclinical experiments, plus the abdominal aorta. The bladder was excluded from the acquisition field. Renal perfusion was determined by visual assessment of the ^{11}C-PABA transit through the abdominal aorta after the injection. The images were

RESULTS

Animal Studies

Whole-body dynamic PET of rats showed that ^{11}C-PABA collected rapidly in the kidneys and was eliminated through the bladder. Minimal signal was observed in other organs. Visual assessment of the PET signal showed renal perfusion, followed by a gradual accumulation of the radiotracer in the renal cortex and a subsequent transition of activity into the collecting system (Figs. 1A and 1B). The time–activity curve (renogram) demonstrated a T_{max} of 8.5 ± 3.9 min in both kidneys, followed by a rapid transit into the pelvicalyceal system, with a $T_{1/2}$ of 32.2 ± 13.1 min. The differential uptake was 49% ± 3.1% and 50.9% ± 3.1% in the right and left kidneys, respectively. As would be predicted, the excretion phase correlated with increased uptake in the bladder (Fig. 1C). The postmortem tissue biodistribution of ^{11}C-PABA and ^{99m}Tc-MAG3 was directly compared by measuring organ-associated radioactivity 30 min after simultaneous injection of both radiotracers in the same animals (Fig. 2). Uptake in background tissue was lower for ^{11}C-PABA than for ^{99m}Tc-MAG3.

In healthy rabbits, ^{11}C-PABA PET also demonstrated high radiotracer excretion through the kidneys and low uptake in background organs. Visual assessment of the renal perfusion showed an accumulation of radiotracer in the cortex starting 3 min after injection, with a later transition into the pelvicalyceal system (Figs. 3A and 3B). Time–activity curves demonstrated a T_{max} of 8.2 ± 1.3, a $T_{1/2}$ of 36.5 ± 11.6 min, and a relative renal uptake of 50.7% ± 1.8% and 49.3% ± 1.8% for the right and left kidneys, respectively (Fig. 3C).

FIGURE 3. ^{11}C-PABA PET/CT renal imaging in healthy rabbits. (A) Coronal dynamic ^{11}C-PABA PET/CT images of right kidney of representative rabbit show rapid delineation of renal cortex and then accumulation in pelvicalyceal system. (B) Maximum-intensity-projection ^{11}C-PABA PET/CT image at 20 min shows similar uptake in left and right kidneys, with low background signal in other organs. (C) Average ^{11}C-PABA time–activity curves for kidneys. Data are mean ($n = 2$). %ID = percentage injected dose.

Dosimetry

The calculated time-integrated activity coefficients are shown in Supplemental Table 1. The time-integrated activity coefficients were longest for the bladder wall and contents. The urinary bladder, followed by the kidneys and lungs, received the highest absorbed dose (Supplemental Fig. 1; Supplemental Table 2). The absorbed dose for the urinary bladder wall was 0.05 ± 0.01 mGy/MBq. The effective dose was estimated to be 0.0039 ± 0.0006 mSv/MBq.

First-in-Humans Study

There were no adverse or clinically detectable pharmacologic effects in any human subject. All had a normal glomerular filtration rate (Table 1). No renal anatomic abnormalities were found. The dynamic PET maximum-intensity-projection acquisition for a representative subject is shown in Supplemental Video 1. ^{11}C-PABA rapidly localized to the kidneys, with minimal signal in other surrounding structures in the same field. The abdominal aorta and renal arteries were detected starting 20 s after injection, with a T_{max} of 24.1 ± 7.6 s (Fig. 4A). The activity gradually accumulated in the renal cortex, reaching a maximal parenchymal uptake at 3.0 ± 0.4 min (Fig. 4B). The T_{max} for the right and left renal pelvises was 9.4 ± 5.4 min (Supplemental Fig. 2). The $T_{1/2}$ for the renal cortex was 23.3 ± 7.5 min, and the average cortical uptake over all time points was $50.9\% \pm 4.3\%$ and $49.06\% \pm 4.3\%$ in the right and left kidneys, respectively.

DISCUSSION

The use of PET for renal imaging is an emerging field that has several key advantages over single-photon imaging in the evaluation of structural abnormalities and in quantification of function (2,6). Among these advantages are better spatiotemporal resolution and absolute camera-based quantification (4). In addition, time-of-flight technology and improved reconstruction algorithms may allow for a decrease in the amount of injected radioactivity. Moreover, PET enables a precise elimination of background activity from surrounding organs (e.g., from the major vessels), and threshold-based approaches can be used to define the activity in the cortex and renal collecting system. Conversely, for renal scintigraphy as opposed to PET, volumes of interest normally cover the entire kidneys to generate a renogram (4). Taken together, these advantages of PET radiopharmaceuticals for renal functional assessment might constitute a clinical benefit. For instance, common γ-emitting agents may underestimate the relative functional performance of one of the kidneys (e.g., malrotation of a single kidney, which can affect the ability to donate a kidney for transplantation) (22). Other clinical applications may include monitoring of therapy-induced renal remodeling, such as after abdominal radiation therapy (23). Renal parenchymal loss can be either diffuse or focal and can occur even at low doses, such as 10 Gy. PET-derived volumes of interest that cover areas at risk in the renal cortex or medulla may allow monitoring of renal injury after radiation or may even have predictive potential before therapy. Given these benefits, several PET radiotracers have shown promise for renal imaging (2,7). With the benefit of a longer physical half-life, ^{18}F-fluorodeoxysorbitol has also been recently evaluated as a potential renal imaging agent (as a replacement for ^{99m}Tc-diethylenetriaminepentaacetic acid) in healthy and diseased rats and in healthy humans (24–26). Compared with ^{99m}Tc-diethylenetriaminepentaacetic acid, the tubular-function–reflecting radiotracer ^{99m}Tc-MAG3 has a more efficient extraction fraction (twice that of ^{99m}Tc-diethylenetriaminepentaacetic acid), which renders it the preferred imaging agent in patients with suspected obstruction and impaired renal function (27). Not surprisingly, ^{99m}Tc-MAG3 is the radiotracer of choice in clinical routine and is used in approximately 70% of the scans in the United States (27). However, recent years have witnessed an expanded use of PET, given its advantages over SPECT (28,29). Thus, PET agents with the potential to replace ^{99m}Tc-MAG3 are needed.

The exclusive renal excretion of PABA has been previously used to assess 24-h urine tests. Although PABA is metabolized
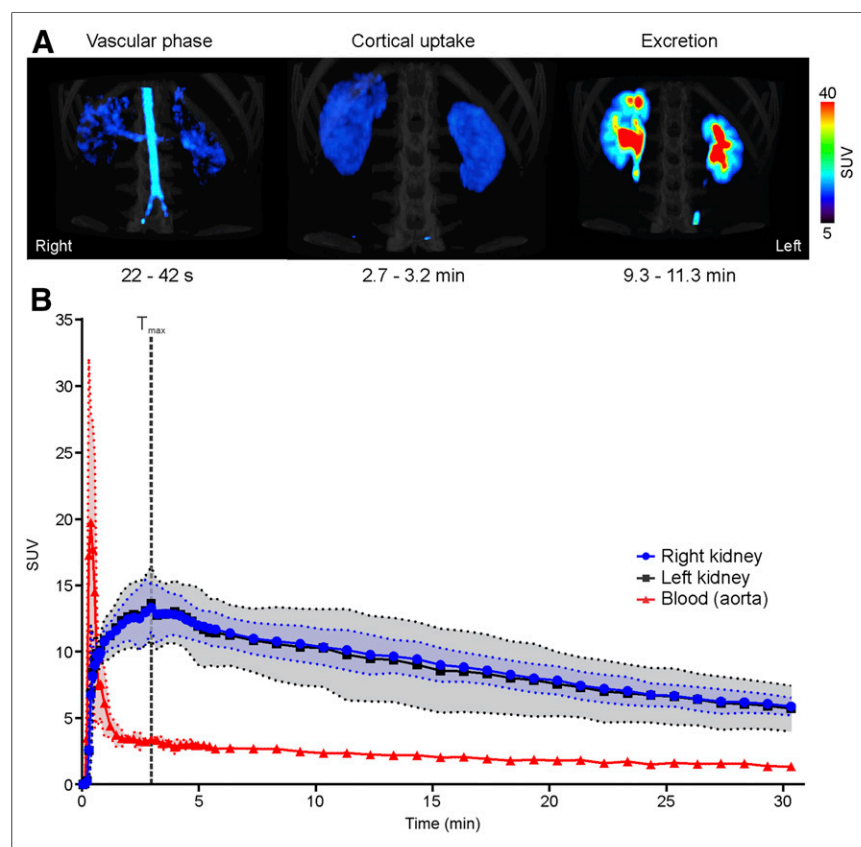

FIGURE 4. ^{11}C-PABA PET renal imaging in healthy human subjects. (A) Maximum-intensity-projection ^{11}C-PABA PET/CT images of representative subject. Vascular phase is observed starting 22 s after injection, demonstrating renal perfusion. Cortical uptake phase is evident within 2.7 and 3.2 min, with maximal parenchymal uptake in renal cortex. Excretory phase is seen after 9 min, indicating maximal uptake in pelvicalyceal system. (B) Average ^{11}C-PABA time–activity curves for kidneys and blood (aorta). Data are mean (solid lines) and SD (shaded areas) ($n = 3$).

by the liver, all its metabolites are also renally excreted (*9,10*). In fact, one of its main metabolites, *para*-aminohippuric acid, has been used as a gold standard to measure effective renal plasma flow because of its high renal tubular secretion, as well as active glomerular filtration once it enters the kidneys (*30*). Radiolabeling PABA with ^{11}C provides high-quality dynamic images of the kidneys while reducing the radiation exposure due to the short biologic and physical half-lives of PABA and ^{11}C, respectively, enabling use in young children. ^{11}C-PABA PET renal imaging in 2 different mammalian models (rats and rabbits) showed rapid localization of the radiotracer in the kidneys with low background signal from other organs. A murine data-based human dosimetry analysis of ^{11}C-PABA showed an effective dose 1.6 times lower than that of ^{99m}Tc-MAG3 (*1*). On the basis of these results, we performed a first-in-humans ^{11}C-PABA PET study on 3 healthy subjects. The near-perfect split renal function observed in the small-animal models and human subjects without known underlying renal disease suggests the potential of ^{11}C-PABA to detect unilateral renal disease or obstruction.

Although clinical implementation of ^{11}C-PABA would be limited to locations with an on-site cyclotron, the intrinsic low radiation exposure of ^{11}C-PABA is particularly well suited to pediatric populations. However, further preclinical and clinical studies are required to understand the potential use of this radiotracer in specific conditions. The present feasibility study has limitations. Patients were not encouraged to drink water before the PET scan, and a specific amount of water was not administered during the study. Further, although the first-in-humans results are encouraging, a larger number of subjects is needed to confirm these preliminary findings.

CONCLUSION

We describe a novel ^{11}C-based tracer used for PET renal functional imaging. In healthy rats, rabbits, and humans, ^{11}C-PABA demonstrated rapid renal excretion with a very low background signal. These results suggest that ^{11}C-PABA might be used as an imaging radiotracer to evaluate renal kinetics and anatomy, providing high-quality images of the kidneys with low radiation exposure compared with the standard of care (SPECT and planar imaging).

DISCLOSURE

ACKNOWLEDGMENTS

KEY POINTS

QUESTION: What is the value of using ^{11}C-PABA for PET renal imaging?

PERTINENT FINDINGS: In healthy rats and rabbits, dynamic PET demonstrated a rapid accumulation of ^{11}C-PABA in the renal cortex, followed by rapid excretion through the pelvicalyceal system. In humans, ^{11}C-PABA PET was safe and well tolerated. The cortex was delineated on PET, and the activity gradually transited to the medulla and then pelvis with high spatiotemporal resolution.

IMPLICATIONS FOR PATIENT CARE: These findings argue in favor of using ^{11}C-PABA as a novel imaging radiotracer to evaluate renal kinetics and anatomy, providing high-quality images of the kidneys with low radiation exposure compared with the standard of care (SPECT and planar imaging).

REFERENCES

1. Blaufox MD, De Palma D, Taylor A, et al. The SNMMI and EANM practice guideline for renal scintigraphy in adults. *Eur J Nucl Med Mol Imaging.* 2018;45:2218–2228.
2. Werner RA, Chen X, Lapa C, et al. The next era of renal radionuclide imaging: novel PET radiotracers. *Eur J Nucl Med Mol Imaging.* 2019;46:1773–1786.
3. Pathuri G, Sahoo K, Awasthi V, Gali H. Renogram comparison of p-[18F]fluorohippurate with o-[125I]iodohippurate and [99mTc]MAG3 in normal rats. *Nucl Med Commun.* 2011;32:908–912.
4. Hofman MS, Hicks RJ. Gallium-68 EDTA PET/CT for renal imaging. *Semin Nucl Med.* 2016;46:448–461.
5. Lipowska M, Jarkas N, Voll RJ, et al. Re(CO)₃([18F]FEDA), a novel ^{18}F PET renal tracer: radiosynthesis and preclinical evaluation. *Nucl Med Biol.* 2018;58:42–50.
6. Szabo Z, Xia J, Mathews WB, Brown PR. Future direction of renal positron emission tomography. *Semin Nucl Med.* 2006;36:36–50.
7. Szabo Z, Alachkar N, Xia J, Mathews WB, Rabb H. Molecular imaging of the kidneys. *Semin Nucl Med.* 2011;41:20–28.
8. Normand G, Lemoine S, Le Bars D, et al. PET [11C]acetate is also a perfusion tracer for kidney evaluation purposes. *Nucl Med Biol.* 2019;76-77:10–14.
9. Bingham S, Cummings JH. The use of 4-aminobenzoic acid as a marker to validate the completeness of 24 h urine collections in man. *Clin Sci (Lond).* 1983;64:629–635.
10. Jakobsen J, Pedersen AN, Ovesen L. Para-aminobenzoic acid (PABA) used as a marker for completeness of 24 hour urine: effects of age and dosage scheduling. *Eur J Clin Nutr.* 2003;57:138–142.
11. Lebel S, Nakamachi Y, Hemming A, Verjee Z, Phillips MJ, Furuya KN. Glycine conjugation of para-aminobenzoic acid (PABA): a pilot study of a novel prognostic test in acute liver failure in children. *J Pediatr Gastroenterol Nutr.* 2003;36:62–71.
12. Tabor CW, Freeman MV, Baily J, Smith PK. Studies on the metabolism of para-aminobenzoic acid. *J Pharmacol Exp Ther.* 1951;102:98–102.
13. Ordonez AA, Weinstein EA, Bambarger LE, et al. A systematic approach for developing bacteria-specific imaging tracers. *J Nucl Med.* 2017;58:144–150.
14. Mutch CA, Ordonez AA, Qin H, et al. [11C]Para-aminobenzoic acid: a positron emission tomography tracer targeting bacteria-specific metabolism. *ACS Infect Dis.* 2018;4:1067–1072.
15. Zhang Z, Ordonez AA, Wang H, et al. Positron emission tomography imaging with 2-[18F]-p-aminobenzoic acid detects *Staphylococcus aureus* infections and monitors drug response. *ACS Infect Dis.* 2018;4:1635–1644.
16. Holt DP, Kalinda AS, Bambarger LE, Jain SK, Dannals RF. Radiosynthesis and validation of [carboxy-11C]4-aminobenzoic acid ([11C]PABA), a PET radiotracer for imaging bacterial infections. *J Labelled Comp Radiopharm.* 2019;62:28–33.
17. Stabin MG, Sparks RB, Crowe E. OLINDA/EXM: the second-generation personal computer software for internal dose assessment in nuclear medicine. *J Nucl Med.* 2005;46:1023–1027.

18. Bolch WE, Eckerman KF, Sgouros G, Thomas SR. MIRD pamphlet no. 21: a generalized schema for radiopharmaceutical dosimetry—standardization of nomenclature. *J Nucl Med.* 2009;50:477–484.

19. Keenan MA, Stabin MG, Segars WP, Fernald MJ. RADAR realistic animal model series for dose assessment. *J Nucl Med.* 2010;51:471–476.

20. Basic anatomical and physiological data for use in radiological protection: reference values—a report of age- and gender-related differences in the anatomical and physiological characteristics of reference individuals. ICRP publication 89. *Ann ICRP.* 2002;32:5–265.

21. Rowe SP, Solnes LB, Yin Y, et al. Imager-4D: new software for viewing dynamic PET scans and extracting radiomic parameters from PET data. *J Digit Imaging.* 2019;32:1071–1080.

22. Weinberger S, Baeder M, Scheurig-Muenkler C, et al. Optimizing scintigraphic evaluation of split renal function in living kidney donors using the geometric mean method: a preliminary retrospective study. *J Nephrol.* 2016;29:435–441.

23. Maturen KE, Feng MU, Wasnik AP, et al. Imaging effects of radiation therapy in the abdomen and pelvis: evaluating "innocent bystander" tissues. *Radiographics.* 2013;33:599–619.

24. Wakabayashi H, Werner RA, Hayakawa N, et al. Initial preclinical evaluation of ^{18}F-fluorodeoxysorbitol PET as a novel functional renal imaging agent. *J Nucl Med.* 2016;57:1625–1628.

25. Werner RA, Wakabayashi H, Chen X, et al. Functional renal imaging with 2-deoxy-2-^{18}F-fluorosorbitol PET in rat models of renal disorders. *J Nucl Med.* 2018;59:828–832.

26. Werner RA, Ordonez AA, Sanchez-Bautista J, et al. Novel functional renal PET imaging with ^{18}F-FDS in human subjects. *Clin Nucl Med.* 2019;44:410–411.

27. Taylor AT. Radionuclides in nephrourology, part 1: radiopharmaceuticals, quality control, and quantitative indices. *J Nucl Med.* 2014;55:608–615.

28. Rowe SP, Gorin MA, Pomper MG. Imaging of prostate-specific membrane antigen using [^{18}F]DCFPyL. *PET Clin.* 2017;12:289–296.

29. Werner RA, Chen X, Rowe SP, Lapa C, Javadi MS, Higuchi T. Moving into the next era of PET myocardial perfusion imaging: introduction of novel ^{18}F-labeled tracers. *Int J Cardiovasc Imaging.* 2019;35:569–577.

30. Juillard L, Janier MF, Fouque D, et al. Dynamic renal blood flow measurement by positron emission tomography in patients with CRF. *Am J Kidney Dis.* 2002; 40:947–954.